Principles of Nuclear Medicine Imaging

6

Aaron J. Krill and Christopher J. Palestro

Nuclear medicine imaging makes use of compounds labeled with small quantities of radioactivity, called tracers, that emit gamma rays detected by a gamma camera. All the nuclear medicine procedures utilized by pediatric urologists provide valuable diagnostic and functional information. Renal perfusion can be quantified which allows for accurate estimates of glomerular filtration rate (GFR). The renal cortex can be imaged very precisely, and any areas of decreased or absent tracer uptake that would signify hypoperfusion from acute pyelonephritis, renal dysplasia, or renal cortical scarring are clearly shown. Renal handling and clearance of radiotracer can also be used to estimate split, or differential, renal function and urinary drainage and can aid in the diagnosis of obstruction. Ischemia associated with testicular torsion can be differentiated from inflammation. The one procedure that fails to provide functional information is direct radionuclide cystography (DRC) which, however, offers a method to detect vesicoureteral reflux that is comparable to fluoroscopic voiding cystourethrography (VCUG) (Table 6.1).

The success of radionuclide renal imaging depends on several factors, including: (1) plasma protein binding and thus volume of distribution of the tracer; (2) rapid delivery to and selective uptake of the tracer by the target organ, e.g., the kidneys, versus the "background"; (3) photon attenuation by fluid collections and surrounding organs; (4) renal function; and (5) technical aspects such as selection of the region of interest (the organs to be evaluated) as well as selection of an appropriate background area.

In general, radionuclide image resolution is diminished compared to, while the radiation dose is similar or often lower than other radiologic imaging modalities such as the conventional VCUG, intravenous pyelography (IVP), and CT scanning. Unlike standard radiology, radiation

Table 6.1 Common uses of nuclear studies in pediatric urology

Estimation of renal plasma flow (GFR/global renal function)
Evaluation of renal cortical lesions (pyelonephritis, scarring)
Estimation of differential renal function (DRF)
Evaluation of urinary drainage, diagnosis of renal obstruction
Evaluation and surveillance of vesicoureteral reflux
Determination of testicular blood flow in cases of suspected testicular torsion

A.J. Krill, MD (✉)
Division of Urology, Department of Surgery,
Virginia Commonwealth University Medical Center,
1200 East Broad St., Suite 7205, 980118,
Richmond, VA 23298-0118, USA
e-mail: akrill@mcvh-vcu.edu

C.J. Palestro, MD
Department of Radiology,
Hofstra North Shore-LIJ School of Medicine,
Hempstead, NY, USA

Division of Nuclear Medicine and Molecular Imaging,
North Shore Long Island Jewish Health System,
270-05 76th Ave., Manhasset & New Hyde Park,
NY 11040, USA
e-mail: palestro@lij.edu

L.S. Palmer, J.S. Palmer (eds.), *Pediatric and Adolescent Urologic Imaging*,
DOI 10.1007/978-1-4614-8654-1_6,

dosage depends primarily on the amount of radioactivity administered. Patient exposure is independent of the number of images obtained, and this allows for almost unlimited "real-time" dynamic imaging which can be important when determining time-dependent processes, such as sporadic vesicoureteral reflux or renal drainage. Administered activity (radiotracer dosage) guidelines can be found in the Society of Nuclear Medicine website (www.snm.org).

Radiopharmaceuticals

Radiopharmaceuticals for evaluation of the kidneys are classified into three general categories: cortical agents, tubular agents, and glomerular agents.

Cortical Agents

^{99m}Tc-Dimercaptosuccinic acid (DMSA) is extensively bound to plasma proteins (90 %), and very little is taken up by red blood cells (0–5 %) [1]. A small amount is glomerularly filtered [2, 3], but this tracer accumulates predominantly in the proximal convoluted tubules. Up to half of the injected activity is retained in the kidneys at 2 h and 70 % at 24 h postinjection [1, 4]. The highest-quality images are obtained about 2–4 h postinjection. These characteristics of DMSA make it an ideal imaging agent for the renal cortex to detect and define pyelonephritis, and renal cortical scarring and to assess the size, shape, and position of the kidneys, and to provide a reasonable estimate of split renal function. Due to its complex renal clearance, DMSA is not useful for estimating global renal function or GFR [5]. Similarly, it is not useful for evaluating urinary drainage because only a small fraction is eliminated in the urine (6 % at 1 h, 25 % at 14 h) [1]. DMSA has been used to aid in localization of renal ectopia, but abdominopelvic ultrasonography may obviate the need for this [6]. ^{99m}Tc-Glucoheptonate, another agent used for renal cortical imaging, is no longer available.

Tubular Agents

These agents are excreted principally through the tubules.^{99m}Tc-Mercaptoacetyltriglycine (MAG3) is the only approved tubular agent available for use in the United States. It is largely bound to plasma proteins (up to 90 %) with minimal (1–2.3 %) binding to red blood cells. This results in a significantly reduced volume of distribution and a high target to background ratio which translates into improved image quality and increased utility in younger patients [7–9].^{99m}Tc-MAG3 is rapidly extracted and secreted by the proximal renal tubules, in a manner qualitatively similar to that of orthoiodohippurate. Renal uptake is reduced by poor function. Up to 70 % of the injected dose is eliminated within 30 min, and by 3 h, up to 90 % can be recovered in the urine [7, 10]. ^{99m}Tc-MAG3 can be used quantitatively or qualitatively for evaluating obstructive uropathy, renovascular hypertension, and renal allografts and has been used to approximate effective renal plasma flow (ERPF) measurement. However, ^{99m}Tc-MAG3 slightly underestimates split renal function when compared directly to ^{99m}Tc-DMSA. This effect was magnified when there was a large difference in function between kidneys but never exceeded 4.3 % [11]. Some authors also have used it for cortical imaging [12, 13].

Glomerular Agents

^{99m}Tc-Diethylenetriaminepentaacetic acid (DTPA) is excreted predominantly by glomerular filtration and can be used to measure GFR. Like ^{99m}Tc-MAG3, ^{99m}Tc-DTPA can be used to assess renal blood flow and function, renal allografts, suspected renovascular hypertension, and obstructive uropathy [14, 15]. Its renal extraction fraction, however, is only about 20 %, compared to 40–50 % for ^{99m}Tc-MAG3 (K). Renal excretion is significantly affected by reduced renal function and performs inferior to ^{99m}Tc-MAG3 in patients with poor renal function and in suspected obstruction [16, 17]. It is not a good agent for renal cortical imaging because of its relatively rapid excretion.

Iodine-125 iothalamate is used exclusively for the nonimaging assessment of GFR. The glomerular agents ^{131}I-orthoiodohippurate and ^{123}I-orthoiodohippurate, once the mainstay of radionuclide renal studies, are no longer available in the United States.

Radiation Dosimetry

In recent years, much has been written regarding radiation dose limitation, specifically the concept of "ALARA – as low as reasonably achievable." This has led authors to favor imaging modalities that do not utilize ionizing radiation whenever possible, such as ultrasonography or magnetic resonance imaging. In situations where this is not feasible or when US or MRI does not perform as well as nuclear or radiographic studies, one needs to choose the study that offers the greatest diagnostic information and with the least radiation exposure.

The majority of nuclear studies, with the exception of cystography, carry a significant radiation burden (Table 6.2). In most cases, nuclear medicine studies used in pediatric urology offer similar or less radiation than other comparable imaging modalities. An exception would be scrotal scintigraphy, whose nonnuclear imaging counterpart is Doppler. ^{99m}Tc-DMSA renal cortical imaging, because of its selective tubular uptake and delayed excretion, provides one of the higher effective radiation doses. This is similar to that of IVP but offers greater sensitivity and specificity [18]. Radionuclide cystography, due to the relatively short period of time and distribution limited mostly to the bladder, provides a much lower effective dose [19] than contrast voiding cystourethrography (VCUG). However, strides have been made in reducing the radiation exposure during VCUG by limiting fluoroscopy time and technical refinements of the instrumentation. The use of grid-controlled pulsed fluoroscopy decreases radiation doses across all age groups by 10–50 % compared to continuous fluoroscopy with an effective dose comparable to that of DRC [19, 20].

GFR Measurement

Traditionally, GFR has been determined by clearance of a substance that is (1) completely filtered by the glomerulus; (2) not synthesized, destroyed, reabsorbed, or secreted by the renal tubule; (3) physiologically inert; and (4) not bound to plasma

Table 6.2 Estimated total body radiation dosimetry (effective dose) for various radiologic and nuclear imaging studies

	Effective dose (mSv) 1 year of age	Effective dose (mSv) 5 years of age	Effective dose as a percentage of total annual atmospheric radiation exposure (%)
^{99m}Tc-**DMSA** cortical scintigraphy	0.8–0.9[a,b]	0.8–0.93[a,b]	25–3
^{99m}Tc-**MAG3** diuretic renography/ indirect radionuclide cystography	0.6–0.77[a,c]	0.6–1.49[a,c]	19–51
^{99m}Tc-**Pertechnate** direct radionuclide cystography	0.08[c]		2.5
^{99m}Tc-**Pertechnate** scrotal scintigraphy *without thyroid blockade*	1.4–1.9[a,c]	1.4–1.9[a,c]	45–61
Intravenous pyelogram (**IVP**) *with grid*	1.0[b]	1.2[b]	32–38
Voiding cystourethrogram (**VCUG**)	0.45–0.89[d,e]	0.45–0.72[d,e]	14–28
Voiding cystourethrogram (**VCUG**) *with GCPL*	0.053–0.069[d]		1.7–2.2

[a]Gadd et al. [88]
[b]Smith et al. [18]
[c]Stabin [19]
[d]Fotakis et al. [89]
[e]Ward et al. [20]

proteins [21]. Agents such as inulin, urea, and creatinine have been used to measure GFR. While inulin clearance is generally acknowledged as the gold standard, it has limited clinical utility as it must be continuously infused and requires multiple timed blood samples. *^{99m}Tc-DTPA*, however, despite having minimal protein binding, meets the above criteria and requires only one injection [22].

GFR can be estimated via DTPA scintigraphy with serial timed plasma samples or via a camera-only method, which is less cumbersome, requires less time, and does not involve blood sampling. Briefly, DTPA is drawn up into a syringe, a 1-min preinjection measurement of the amount of radioactivity in the syringe is made, it is rapidly injected intravenously, a 1-min postinjection measurement of the empty syringe is made, and serial images of both kidneys are acquired at 1-min intervals between 1 and 3 min postinjection. The 2–3-min interval is the best time for GFR measurement. Both total and fractional GFR can be estimated. The entire duration of the study is less than 10 min.

The camera-only technique was described by Gates who compared DTPA measurements of GFR to 24-h creatinine clearance values obtained for each patient. There was an excellent linear correlation (r^2>0.9) between the two measurements across a wide range (1–113 mL/min) of renal function. The DTPA study was repeated 24–48 h later, and a remarkable correlation coefficient (99 %) with the first study confirmed the technique's reproducibility [23]. Some studies suggest that ^{99m}Tc-DTPA is not reliable for estimating GFR in young children [24, 25]. Chandhoke et al. reported significant inaccuracy in estimation of GFR when compared to clearance of continuously infused iothalamate in children. They postulated that this may be due to the fact that the adult renal depth correction used in the Gates method may not be applicable to children [26].

Renal Cortical Scintigraphy

The very high uptake of ^{99m}Tc-DMSA by the pars recta of the proximal tubules and its minimal glomerular filtration and loss in the urine allows for detailed images of the renal cortex (Fig. 6.1). Traditionally, ^{99m}Tc-DMSA cortical imaging has been used to delineate areas of cortical hypoperfusion that accompany acute pyelonephritis and also to demonstrate renal scarring from prior infections. Lesions associated with acute pyelonephritis appear as areas of photopenia, with preservation of the normal renal contour. In contrast, renal cortical scars appear as

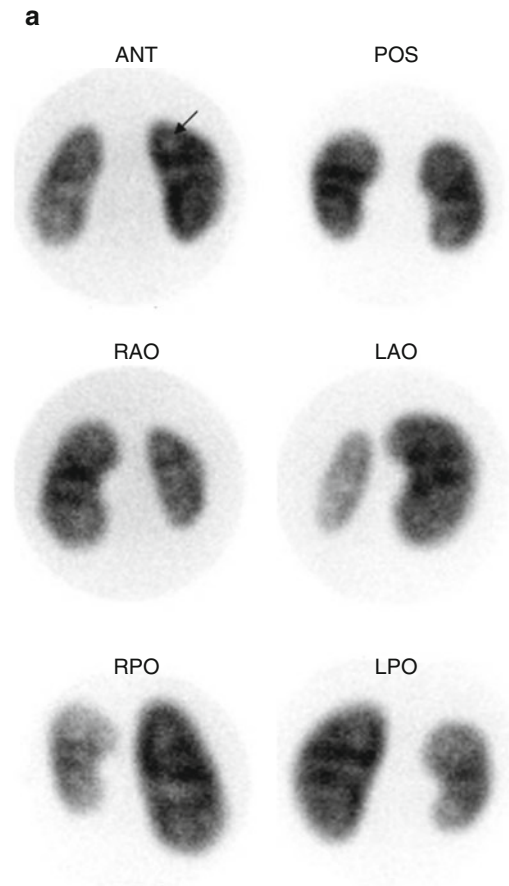

Fig. 6.1 Normal DMSA renal cortical study. (**a**) There is homogeneous distribution of activity throughout both kidneys on the pinhole images. The discrete round areas of decreased activity (*arrow*) are the calyces. The pinhole collimator distorts apparent organ size, which is why in some of the views, one kidney appears larger than the other. The coronal SPECT images (**b**) demonstrate homogeneous distribution of activity throughout the cortex of both kidneys. Note that unlike their appearance on the pinhole images, the kidneys are similar in size (With respect to the orientation of the SPECT images, the anterior most aspect of the kidneys is in the upper left image, and the posterior most aspect is in the lower right image)

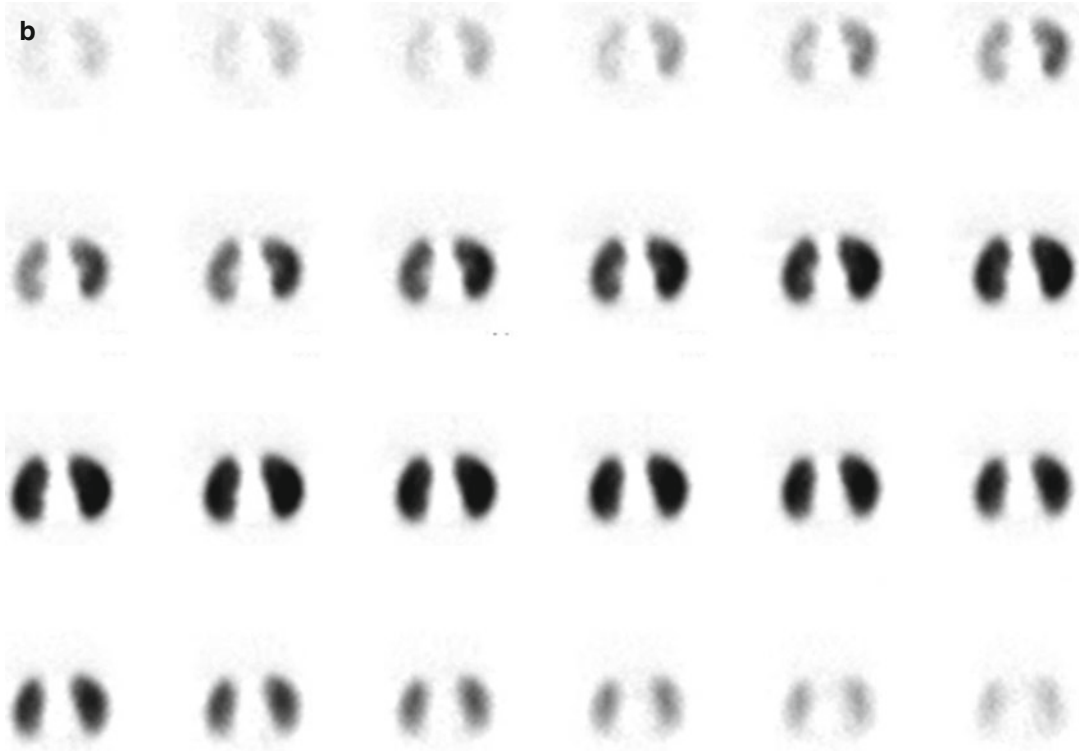

Fig. 6.1 (continued)

wedge-shaped areas of photopenia which distort the renal contour (Fig. 6.2). This information can aid in surgical planning and has been proposed to identify patients who should be screened for vesicoureteral reflux, the so-called top-down approach [27, 28].

^{99m}Tc-DMSA cortical scintigraphy also can provide information about differential renal function (Fig. 6.3). However, because it is filtered to a small degree, and blood clearance occurs over a period of hours, variations in renal DMSA uptake are not always equivalent to true variations in function. Thus, ^{99m}Tc-DMSA should not be used to estimate absolute renal function or GFR [29].

Description of Technique for ^{99m}Tc-DMSA Cortical Scintigraphy

In an effort to standardize reporting and methodology for renal cortical scintigraphy, several consensus statements and procedure guidelines have been issued, but there is still some variation in the timing of image acquisition (1.5–4 h postinjection), the need for sedation, type of views (planar and pinhole magnification vs. SPECT), and reporting of results [30, 31]. For clarity, the described technique is that of the Society of Nuclear Medicine Guideline publication in 1997, with some recent modifications by Zeissman et al. [31]. Single-photon emission computed tomography (SPECT) imaging will be described separately as there is considerable disagreement as to its utility versus standard planar and pinhole magnification images and also serious difficulties in multicenter standardization [31–34].

A large or standard field of view gamma camera equipped with a parallel-hole high-resolution collimator and/or a pinhole collimator with a 4 mm aperture is recommended. The patient is placed supine for parallel-hole imaging and prone for pinhole imaging. Imaging can begin at 1.5–2 h postinjection, although superior image quality is obtained by waiting at least 4 h [31, 35]. Classically, images are acquired in the posterior and the left and right posterior oblique planes.

Differential function is calculated from the posterior planar view using the parallel-hole collimator. Background correction can be undertaken by selecting a region of interest (ROI) around both kidneys in the planar projection and then drawing circumferential background regions approximately 2 pixels in width and 2 pixels away from the kidney. Acquisition time for the images varies by technique, with pinhole magnification requiring fewer counts (150,000 vs. 300,000) but longer acquisition time than the parallel-hole collimator (10 min vs. 5 min). For pinhole images, the kidney should fill approximately 2/3 of the field of view. In cases of significant hydronephrosis, furosemide can be given and/or delayed images can be performed up to 24 h after injection of radiotracer.

Various techniques have been described to adequately image the cortex; most centers rely on pinhole magnification to properly delineate renal scarring and acute pyelonephritis. These images should be correlated with other imaging modalities such as ultrasonography and voiding cystography, when available. A sample grading protocol used in the RIVUR trial is described in Table 6.3 in which the renal cortex is divided into numbered segments and severity graded by the quantity of segments involved [31].

SPECT Versus Standard Planar/ Pinhole Imaging

Single-photon emission computed tomography, or SPECT, provides a panoramic multi-image view of both kidneys versus the standard three views of planar and pinhole magnification. Some suggest that SPECT is more sensitive and easier to interpret than planar and pinhole images. Other disagree contending that SPECT is less specific than planar and pinhole imaging. In an international multicenter survey of nuclear medicine experts, SPECT was performed routinely by only 22 % of respondents and seldom performed by 45 % of respondents and never used by 33 % of the respondents [30]. Further complicating matter is the absence of an accepted standard technique, with several authors reporting a range of projections (60–120) and varying increments of scanning time [35–37].

Interobserver Variability in SPECT and Planar ^{99m}Tc-DMSA Cortical Scintigraphy

^{99m}Tc-DMSA planar imaging has been shown to have excellent interobserver agreement in several reports using various measures. Consensus opinion regarding "normal" and "abnormal" among expert observers was 93.5 % and 90.5 %, respectively [38, 39]. While the reliability and reproducibility of planar and pinhole imaging is well established, little has been published on SPECT

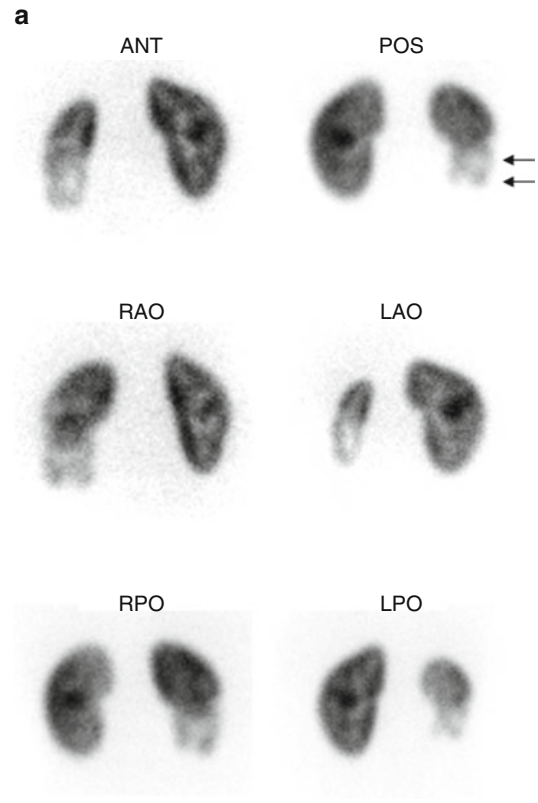

Fig. 6.2 Renal cortical scarring. Pinhole images (**a**) demonstrate an area of decreased tracer uptake with associated cortical volume loss (*arrow*), in the lower pole of the right kidney. On the coronal SPECT images (**b**), the right lower pole abnormality is equally well seen. In addition, the right kidney is smaller than the left

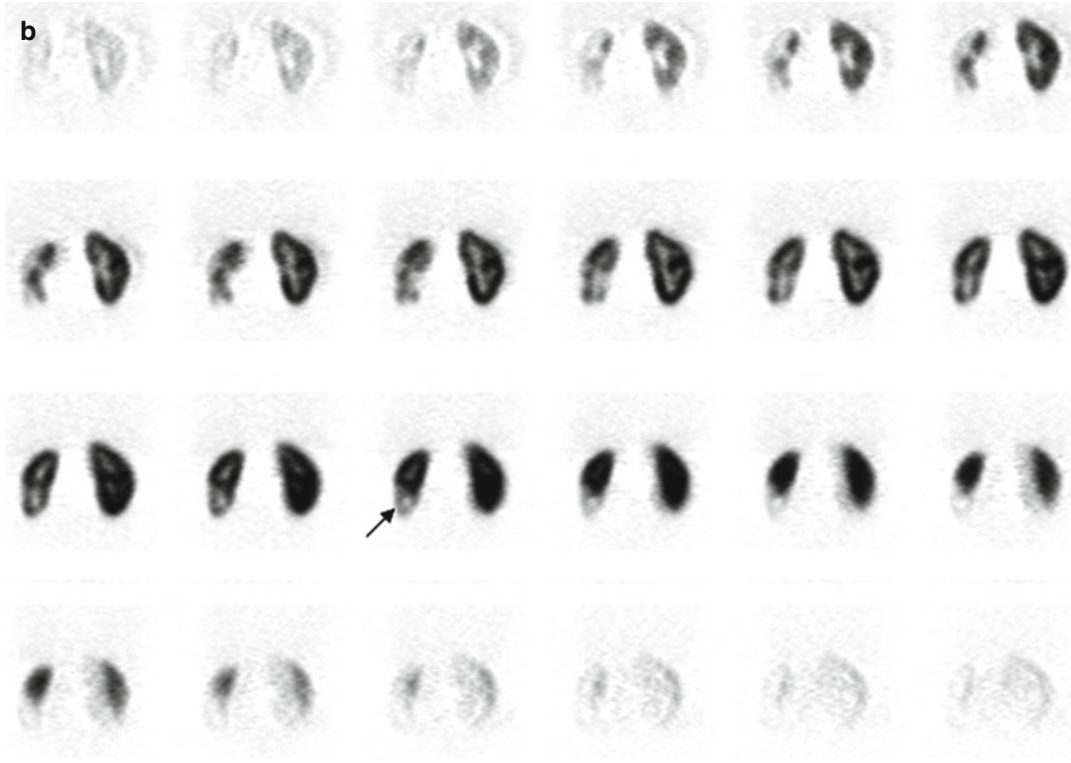

Fig. 6.2 (continued)

interobserver agreement, and the absence of a standard acquisition protocol hinders accurate comparisons among studies. Craig et al. suggest decreased reproducibility and interobserver agreement in interpretation of SPECT images compared to planar images [40]. Cost also can be a factor; by one estimate, SPECT costs up to 36 % more to perform than planar imaging. This is presumably due to longer image acquisition times and a possible greater need for sedation [41].

SPECT Versus Planar/Pinhole Magnification Imaging Animal Models

In comparison to standard planar and pinhole imaging, SPECT is comparable, possibly at the expense of decreased specificity and higher false-negatives. The performance of standard planar and pinhole magnification DMSA cortical imaging in the diagnosis of acute pyelonephritis has been widely investigated, and most authors agree on a sensitivity around 90 % and specificity between 90 and 100 % [42, 43].

Craig et al. report the results of a meta-analysis of published animal trials evaluating the overall ability of ^{99m}Tc-DMSA cortical scintigraphy to diagnose acute pyelonephritis. He initially found an *average sensitivity of 84 %* and an *average specificity of 88 %*; however, after correcting statistical errors and excluding some unusable data, there were no significant difference between SPECT and planar imaging [41].

In one elegantly designed study correlating histopathology and cortical scintigraphy in piglets, Majd et al. directly compared SPECT and pinhole imaging for detection of pyelonephritis 1–10 days after infection. After evaluating all zones of pyelonephritis over the entire time period, SPECT carried a sensitivity of 91 % vs. 86 % for pinhole imaging but was less specific, 82 % vs. 95 % compared to planar imaging.

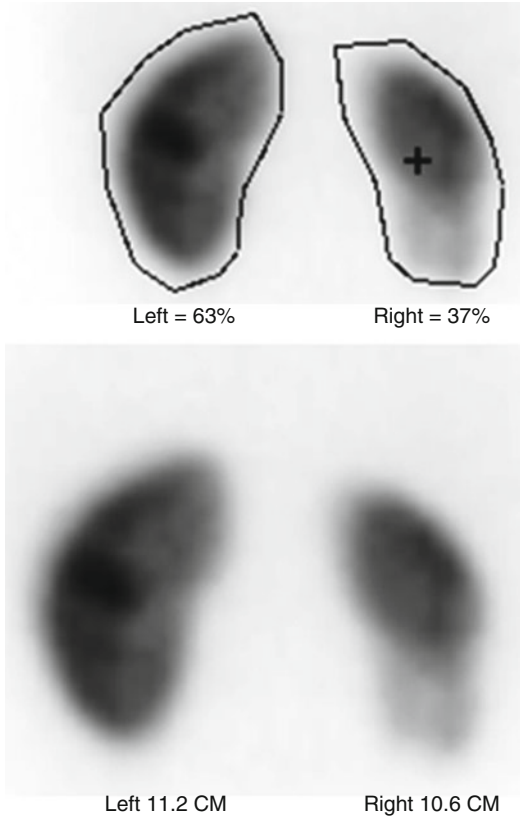

Fig. 6.3 When performing renal cortical scintigraphy, it also is possible to determine differential (split) renal function and to measure renal size

Table 6.3 Sample grading system for renal cortical scarring in ^{99m}Tc-DMSA scans (Zeissman et al. [31])

Grade	Severity	Number of affected renal segments
0	Normal	0
1	Mild	1–2
2	Moderate	3–4
3	Severe	>4
4	Global atrophy	Diffuse scarring

Overall accuracy was similar for both techniques, 88 % for SPECT and 90 % for pinhole imaging (Table 6.4) [42].

Rossleigh et al. compared SPECT to standard planar imaging in the diagnosis of renal cortical scarring in a refluxing piglet model with post-study histopathologic confirmation. Each animal after VCUG-confirmed VUR and ^{99m}Tc-DMSA-confirmed pyelonephritis underwent another planar ^{99m}Tc-DMSA and SPECT scan 3 months later. They reported similar sensitivity, specificity, and overall accuracy between planar images, pinhole magnification, and SPECT (Table 6.5) [34].

SPECT Versus Planar Imaging for Detecting Pyelonephritis

There are several human studies demonstrating the ability of SPECT to detect more renal lesions in acute pyelonephritis and renal cortical scars than planar and pinhole imaging. Tarkington et al. compared the ability of SPECT and pinhole imaging to detect renal cortical defects of various etiologies in 33 children, about 60 % of who did not have UTI, VUR, or prior pyelonephritis. In this heterogeneous population, 63 % of the pinhole image studies read as "normal" were found to have cortical abnormalities on SPECT. They also found that SPECT "clarified or enhanced" the pinhole imaging in 71 % of the kidneys studied. Overall SPECT found 55 % more cortical defects than pinhole imaging [44]. Yen et al. compared SPECT to planar imaging in 27 infants and 17 children upon diagnosis of acute pyelonephritis and at 3 months posttreatment and found SPECT identified significantly more scarring than planar imaging (33 % vs. 9.5 %, $p<0.05$) at

Table 6.4 Detection of acute pyelonephritis in piglets (Majd et al. [42])

	Sensitivity (%)	Specificity (%)	Accuracy (%)
Pinhole magnification	90	95	92
SPECT	96	95	96

Table 6.5 Detection of post-pyelonephritis renal scarring in pigs (Rossleigh et al. [34])

	Sensitivity (%)	Specificity (%)	Accuracy (%)
Pinhole magnification	74	99	92
SPECT	59	98	87

3 months, particularly in the presence of high-grade VUR than those found using planar imaging [36]. The prospective data of Applegate et al. seem to confirm prior human studies that SPECT detects more "definite" lesions than pinhole and planar images. Cortical defects were classified as "possible" or "definite" and "single" or "multiple" as defined by a consensus of three blinded experts. However, they found that no technique was superior for detecting multiple as opposed to solitary defects [32].

SPECT Versus Planar/Pinhole Imaging Summary

Data from studies in human subjects seem to corroborate previous animal studies that demonstrate increased sensitivity with SPECT, but without histopathologic analysis, false-positives cannot be excluded with certainty. As such, the pooled data from the animal studies is slightly less impressive but probably more accurate than that reported in human subjects. Regardless of technique, the performance of ^{99m}Tc-DMSA renal cortical scintigraphy in the diagnosis of acute pyelonephritis and the detection of renal cortical scarring is excellent. At best, SPECT is slightly more sensitive than, and is comparable in specificity to standard pinhole imaging. It seems that the combination of SPECT and pinhole imaging may improve interobserver agreement and may be more useful than either test alone.

Description of Technique for Diuretic Nuclear Renography

In 1992 the Society for Fetal Urology and the Pediatric Nuclear Medicine Council released a consensus statement regarding performance of the "well-tempered diuretic renogram" in response to a lack of standardization of technique and interpretation of dynamic renal imaging. However, this protocol has not been adopted universally, and debate continues regarding such technical aspects as method of pretest hydration, need for urethral catheterization, timing of diuretic administration, and even the method of calculation of urinary drainage [45, 46].

Patient Preparation

The infant kidney continues to mature, and GFR continues to increase for the first year of life which is reflected in the child's ability to clear ^{99m}Tc-MAG3 from the plasma [47]. In general, diuretic renography should be performed after the child is at least 1 month of age to limit spurious prolongation of drainage and a potentially inadequate response to diuretic challenge due to immature renal tubules [46]. Oral hydration is encouraged, and IV hydration is provided as a 15 mL/kg bolus of D5 0.3NS or D5 0.25NS 15 min prior to injection of radiotracer. Maintenance intravenous fluid is provided throughout the study. A urethral catheter for constant bladder drainage decreases the radiation dose to the bladder wall and gonads and also minimizes impedance of antegrade flow of urine from the collecting system simulating delayed drainage.

Renogram Phase

^{99m}Tc-MAG3 is administered intravenously with the child placed in supine position and the gamma camera under the bed. The field of view should include the heart, kidneys, ureters, and the bladder. Digital images are collected at 20 s/frame, and analog images are recorded for 30 min with practitioner preference determining the timing. A typical renogram acquisition is 1- or 2-min image intervals for 30 min (Fig. 6.4).

For accurate estimation of split renal function during the renogram phase, care must be taken when selecting the region of interest (ROI). This can be done manually or with computer assistance in a semiautomated or fully automated fashion. Regardless, the ROI must encompass the entire kidney including the renal pelvis. The background ROI should be approximately 2 pixels wide and encircle the renal ROI. Acquisition time should be a minimum of 20–30 min. To calculate differential renal function (DRF), the total counts of the renogram curve for each kidney minus the background

counts are calculated during the interval from 60 s post tracer injection until the appearance of activity in the collecting system. Usually this is within the first 60–120 s of the study. There are several methods used to estimate DRF, but the two most commonly employed are the *integral method* where area under the renogram curve is calculated and the *Rutland-Patlak plot* which relies on the mean slope of the ascending renogram curve. In most situations, both methods are thought to be equivalent [48].

Controversy exists over the so-called "supranormal" functioning kidney, split renal function of ≥55 % in unilateral hydronephrotic kidneys, which has a prevalence of 4–21 % [49–53]. Various explanations have been proposed, including compensatory hyperfunction, artifact related to background correction [49, 53], or variation in the method of quantification of function [50, 54]. Reports of laterality are variable.

Diuretic Phase

Furosemide at a dose of 1 mg/kg (max 40 mg) for children <1 year and 0.5 mg/kg for children >1 year is given IV after completion of the renogram phase, usually at 20–30 min (F+20–30) or when

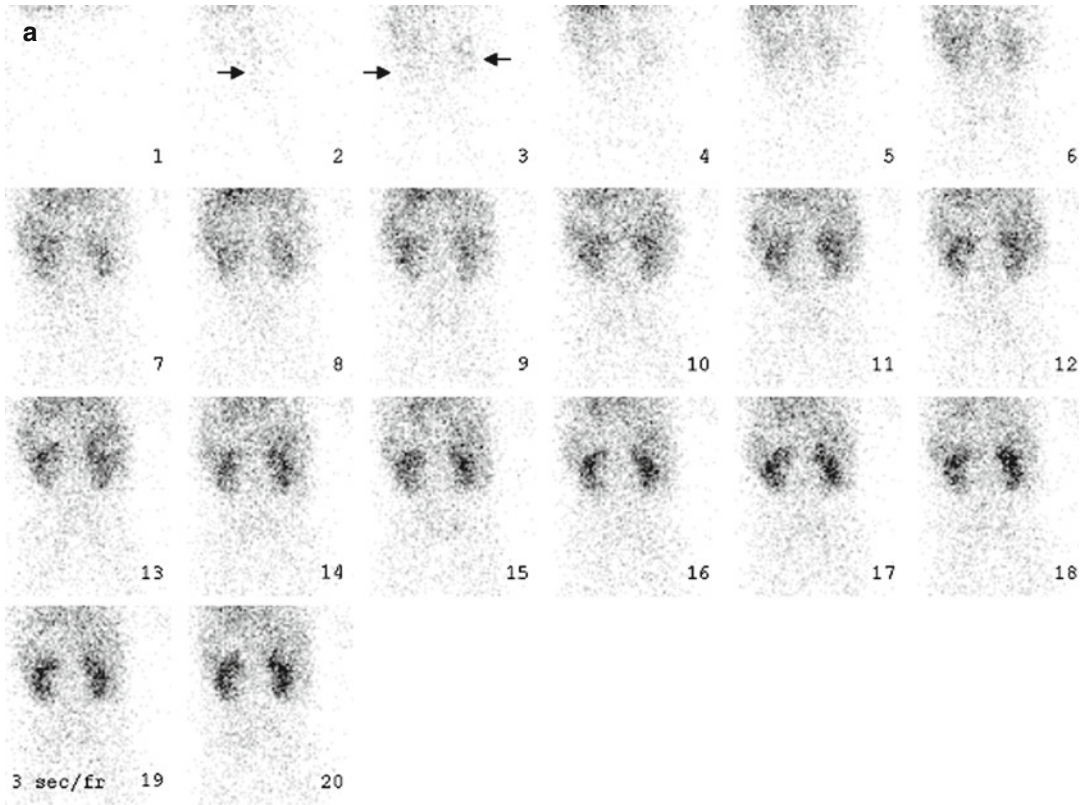

Fig. 6.4 Normal diuretic renography. On the flow phase (**a**) of the study, the abdominal aorta (*arrow*) appears in frame 2. The kidneys (*arrows*) are seen about 3 s later, in frame 3. Visualization of the kidneys within 2–3 s after visualization of the abdominal aorta generally is equated with normal renal perfusion. In the case of the renal transplant (not shown), the kidney should appear within 2–3 s after the iliac artery is seen. On the functional phase (**b**) of the study, the kidneys are similar in size, and there is prompt appearance of activity in the collecting systems and urinary bladder. Adequate hydration is important to the success of diuretic renography. Activity should appear in at least one of the collecting systems within 3–5 min after radionuclide injection. Alternatively bladder activity should appear within 10 min after injection. In this patient, activity is clearly seen in both collecting systems and the urinary bladder on frame 1 or about 3 min after injection

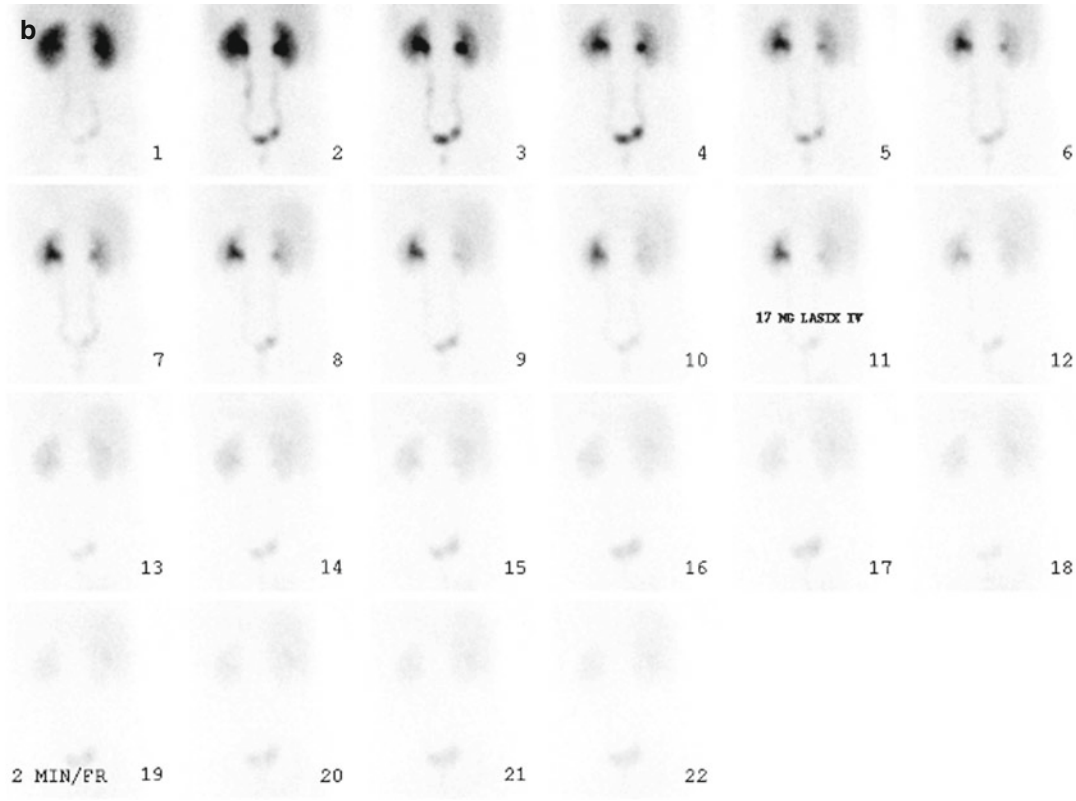

Fig. 6.4 (continued)

the collecting system is thought to be full. Other centers advocate simultaneous administration of tracer and diuretic (F0) in cases of known hydronephrosis [55]. To ensure uniform distribution of radiotracer throughout the collecting system, the child may be placed prone or in the sitting position to maximize drainage. In the setting of hydronephrosis, the ROI for the diuretic time-activity curve should only include the renal pelvis and collecting system. The background ROI should circumscribe the kidney excluding the hilum. For children with hydroureteronephrosis, the ROI for the diuretic time-activity curve should be placed around the dilated renal pelvis with a separate ROI circumscribing the ureter to the level of the UVJ making sure to exclude the urinary bladder.

Computer frame rates are recorded every 20 s for 40 min. Drainage can be calculated by determining the time it takes for half of the tracer activity to leave the collecting system after diuretic administration ($t_{1/2}$ washout), estimating output efficiency (OE), or calculating normalized residual activity (NORA) (Fig. 6.5).

Defining Renal Obstruction

The differentiation of antenatal hydronephrosis from significant renal obstruction that causes deterioration in function is by nature a retrospective diagnosis. Prior to the advent of routine antenatal ultrasound screening, most cases of UPJ or UVJ obstruction were detected later in life when patients developed symptoms. Since the 1970s, antenatal hydronephrosis has been commonly detected via ultrasound. Because this antenatally detected hydronephrosis (presumed urinary obstruction) is asymptomatic in the majority of cases, this poses a diagnostic and therapeutic dilemma for the pediatric urologist. Determining

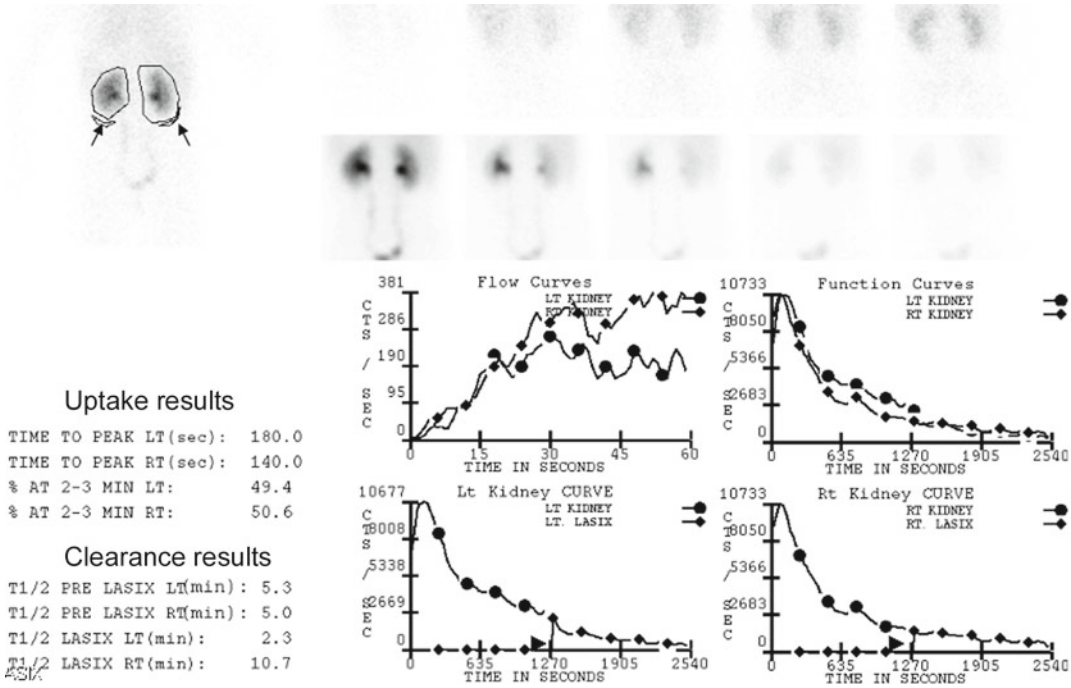

Fig. 6.5 Numeric data from the patient study illustrated in Fig. 6.4. The regions of interest drawn around the kidneys as well as the background regions (*arrows*) are shown in the *upper left image*. The *top left graph* is a representation of renal flow, and the *top right graph* represents renal function. The two graphs below are the individual functional curves of each kidney, with the *vertical bar* (*arrowheads*) indicating the time (approximately 21 min) at which diuretic was administered

which of these patients will require surgery and which will resolve has been challenging.

Historically, several diagnostic tests were used to predict obstruction, including IVP, and direct measures of renal pelvis pressure differentials (Whitaker test). Standard nuclear renograms followed, and renal transit times and/or visual analysis of renogram curves that tracked the passage of radiotracer through the kidney was used to define obstruction. Difficulties with poor image resolution and variations in patient hydration and a significant number of false-negative studies in hydronephrotic patients with delayed renograms without evidence of obstruction limited the usefulness of this technique.

O'Reilly et al. introduced the diuretic renogram (DRG) in the late 1970s in an effort to identify the children with dilated, nonobstructed collecting systems and separate them from children with true obstruction. The analysis of drainage curves was born, and various patterns of drainage were defined. The shape of a normal post-diuretic renal drainage curve was described as brisk and exhibited rapid elimination of tracer (*pattern I*). The "obstructive" pattern (*pattern II*) showed little response to the diuretic with a flat and sometimes rising drainage curve as activity continued to accumulate within the collecting system. A third pattern (*IIIa*) was described which revealed a normal and rapid response to diuretic even after a continually rising or plateau renogram curve. The fourth pattern (*IIIb*), thought to represent obstruction as well, was a rising or plateau renogram curve with no response to diuretic [56, 57].

To further characterize these patients, the concept of $t_{1/2}$ washout, or the time it takes for half of the radiotracer to drain after diuretic injection, was introduced. Three categories were created to stratify patients at risk: $t_{1/2}$ of less than 10 min, definitely normal; $t_{1/2}$ of 10–20 min, indeterminate; and $t_{1/2}$ greater than 20 min,

obstructed (Figs. 6.6 and 6.7). Each of these parameters has significant shortcomings, and none have proven accurate enough to make the definitive diagnosis of obstruction in equivocal cases. Several authors have documented spontaneous resolution of hydronephrosis in children previously thought to be obstructed by drainage curve and $t_{1/2}$ washout [58–60].

Calculation of Halftime of Washout or $t_{1/2}$ Washout

The halftime for elimination of radiotracer beginning at the time of diuretic injection, or $t_{1/2}$ washout, has traditionally been the preferred way to define significant urinary obstruction [46, 61]. It is measured in minutes, with less than 10 min being thought of as normal or nonobstructed, 10–20 min as indeterminate, and greater than 20 min as significantly obstructed. Analysis begins at time *t* when the diuretic is administered, usually 20–30 min after injection of the radionuclide or when the collecting system is seen clearly. There is usually a short plateau and then a rapid decrease in activity that corresponds to diuretic response, which then plateaus as drainage of the radioactivity is completed. The shape of the drainage curve can supply useful information. Flat or rising curves are thought to represent obstruction. Use of the $t_{1/2}$ alone is troublesome, as it depends on several factors, including the state of hydration of the patient, the presence of significant hydronephrosis, and the amount of radioactivity at the time of diuretic injection and at the end point of the drainage phase. For example, in kidneys with

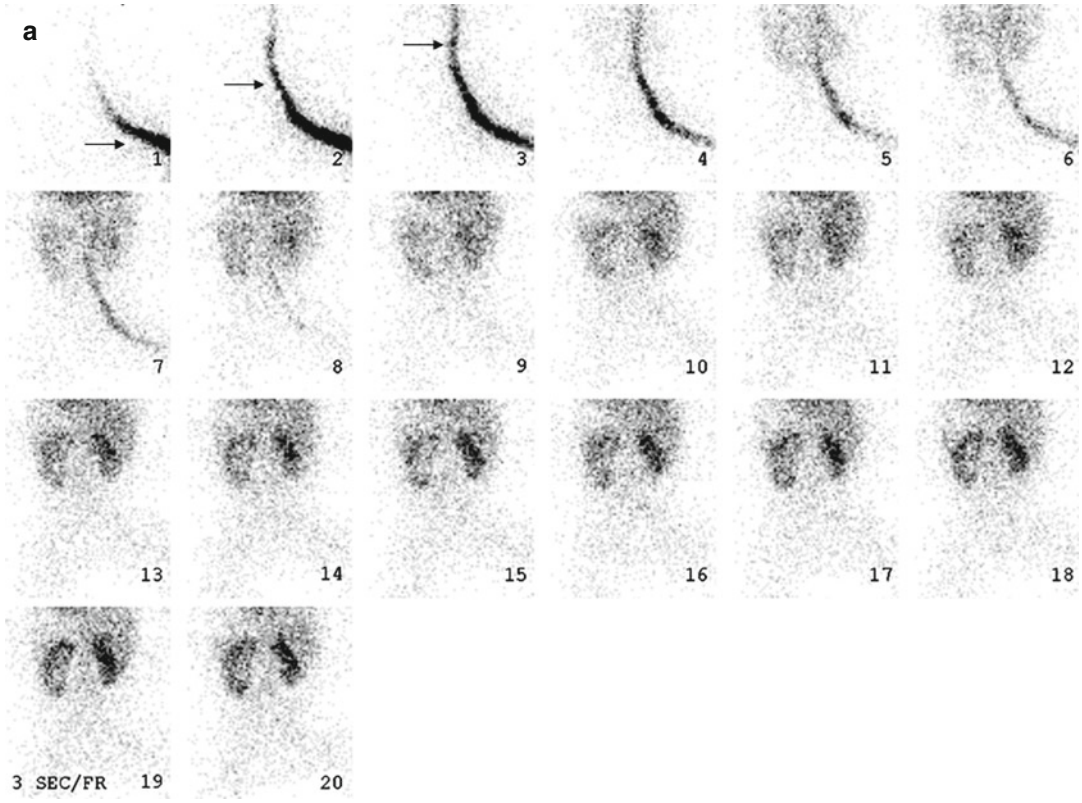

Fig. 6.6 Obstructed left kidney. Flow (**a**) and functional (**b**) images. On the initial images in the flow phase, it appears as if activity is moving retrograde in the aorta (*arrows*). The patient was injected in a lower extremity vein, and this actually is activity ascending through the inferior vena cava. The left kidney is considerably larger than the right. The right collecting system drains spontaneously prior to diuretic challenge, while there is little or no drainage from the left collecting system before or after diuretic challenge

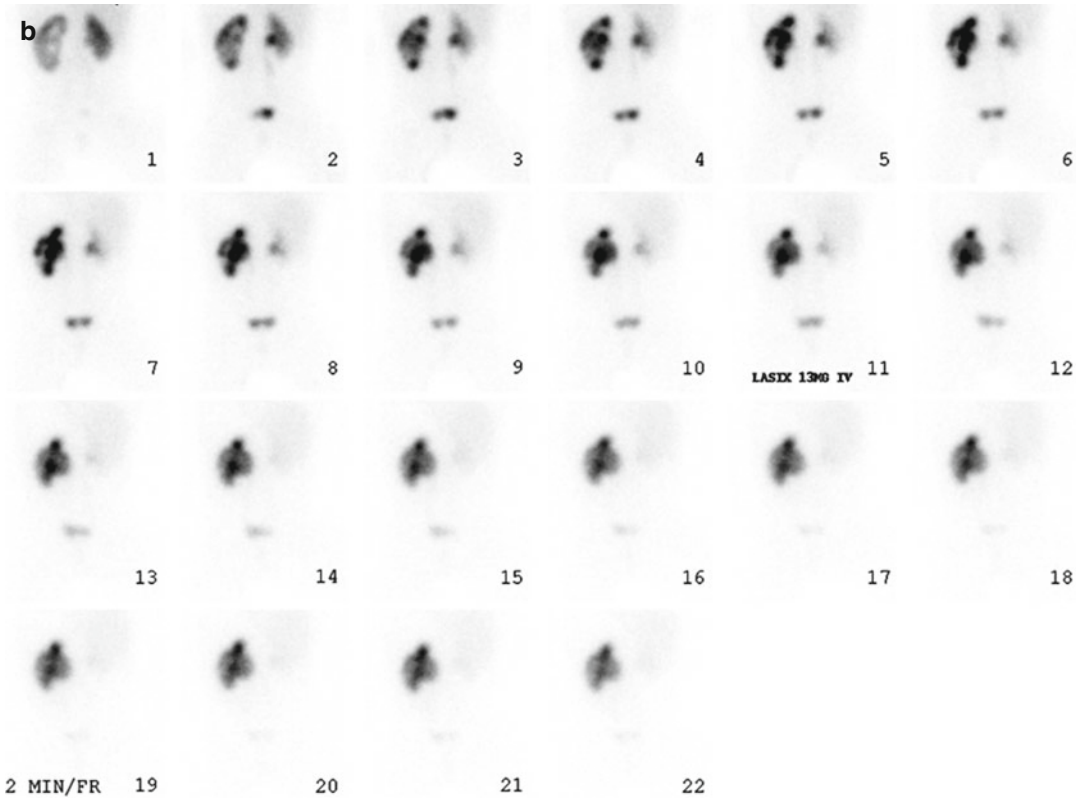

Fig. 6.6 (continued)

normal function with almost complete drainage before the diuretic injection, the drainage curve will be flat and the $t_{1/2}$ washout can be significantly prolonged even though drainage is normal. This underlies the importance of examining the drainage curve and not simply categorizing children by their $t_{1/2}$ washout values alone. As such, $t_{1/2}$ washout values should NOT be reported for kidneys that drain prior to diuretic administration (Fig. 6.7). While the $t_{1/2}$ washout is very useful for excluding obstruction in the setting of normal drainage, there is a significant portion of patients with indeterminate drainage values, and this can lead to diagnostic uncertainty.

Gravity-Assisted Drainage

The standard diuretic renogram is performed with the patient in the supine position. Patients who have nonobstructive significant hydronephrosis and those who have residual atonic renal pelvis after pyeloplasty often exhibit delayed $t_{1/2}$ in the "indeterminate" or "obstructed" range. Several authors suggest that renal drainage can also be positional, with possible improvement in renal drainage upon upright imaging [62, 63]. Wong et al. reported the effects of gravity-assisted drainage (GAD) in a mixed cohort of postoperative pyeloplasties, tapered ureteral reimplants, and children who were managed nonoperatively. GAD was performed by holding the child upright for 5 min after completion of the diuretic phase followed by acquisition of one final image. The upright image was then compared to the last 5 min of the diuretic phase. Using a cutoff value of >50 % residual activity after 5 min of GAD to define obstruction helped to stratify patients with halftimes in the "indeterminate" range. *In patients with a $t_{1/2}$ washout of 10–20 min, sensitivity, specificity, and accuracy for GAD >50 % in defining obstruction*

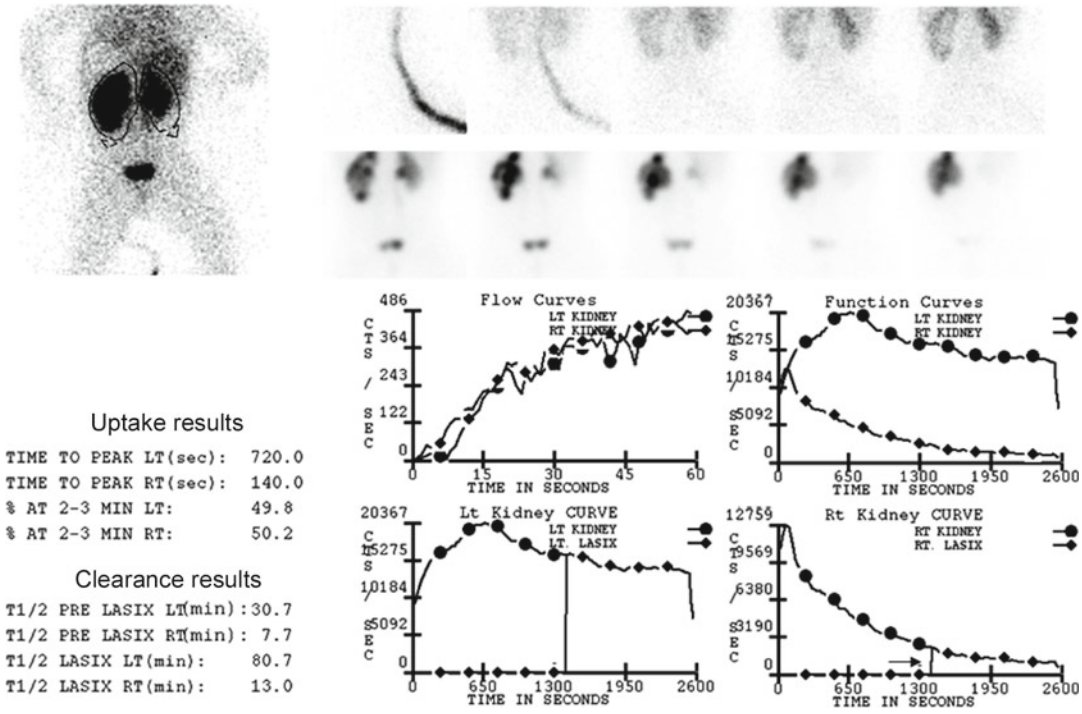

Fig. 6.7 Numeric data from the patient illustrated in Fig. 6.6. The numeric data confirm the visual impression. There is virtually no drainage from the left collecting system at any time during the test. Although the calculated $T_{1/2}$ washout from the left collecting system is 80 min, the curve is nearly flat and we would report this simply as no response to diuretic challenge, consistent with obstruction. Note also that the $T_{1/2}$ washout from the right collecting system is 13 min, which is an equivocal response to diuretic challenge. When the diuretic challenge was given (*arrow*), however, nearly all the activity already had drained from the collecting system, and consequently, this value is not meaningful. We report these situations as spontaneous drainage prior to diuretic challenge and do not report a $T_{1/2}$ washout

were 100 %, 79 %, and 83 %, respectively. In patients with $t_{1/2}$ washout >20 min, sensitivity was 88 %, specificity was 74 %, and accuracy was 84 % [63]. GAD should be a standard component in all diuresis renography studies as it can help clarify and correctly categorize some of those children with indeterminate or equivocal $t_{1/2}$ washout.

Renal Output Efficiency (OE)

Chai defined OE as the total renal output up to a time *t* expressed as a percentage of the total renal input, i.e., the amount of tracer that has left the kidney at a selected time expressed as a percentage of what the kidney has extracted from the blood [64]. OE provides an objective measure of the renal response to diuretic challenge taking into account renal function and thus may be more useful in children with reduced renal function. Images of the left ventricle are used to generate a blood clearance curve which is fitted to the rising phase of a background-corrected whole kidney time-activity curve. This represents the kidney input as a function of time. Post-diuretic background-corrected renal output is then subtracted from input and expressed as a percentage of the corrected renal input. OE can be calculated at any point during the study (time *t*); however, the input images during the first 1–2 min of the study must be used.

An OE for "normal kidneys" is defined as at least *78 % in adults* [64]. Saunders et al. compared OE to DRG in 74 young children (91 renal units) with a median age of 4 months.

Final outcomes were determined by surgical pathology and clinical follow-up. OE was calculated at 20 min post-diuretic injection and after gravity-assisted drainage. The children were initially stratified by DRG findings; obstruction on DRG was defined as at least two of the following: $t_{1/2} > 20$ min, split renal function <40 %, and by visual assessment of a flat or rising post-diuretic drainage curve. Normal OE values were obtained by assessing the non-hydronephrotic contralateral kidney. In non-hydronephrotic kidneys, the mean OE was 96 % compared to 93 % in hydronephrotic but unobstructed kidneys. The *lower limit of normal was defined as 79 %* (2 SD below the mean in hydronephrotic nonobstructed kidneys). $T_{1/2}$ washout on diuretic renography initially stratified the patients as 52 nonobstructed, 20 indeterminate, and 19 obstructed. Using a value of <79 %, OE classified 61 patients as normal and 20 as obstructed. The final diagnosis revealed true obstruction in 22 and no obstruction in 69. This resulted in an *overall diagnostic accuracy for OE of 89 %*. In the indeterminate group, OE correctly classified all cases of obstruction, and 56 % of those found not to be obstructed. Interestingly, OE performed well in a subgroup of patients with reduced differential renal function (mean DRF 32 %) detecting all true cases of obstruction and classifying ~70 % of unobstructed patients correctly. This resulted in a *sensitivity of 100 %, a specificity of 82 %, and an accuracy of 80 % in children with mild to moderate renal dysfunction* [65].

Normalized Residual Activity (NORA)

Normalized residual activity (NORA), first described by Piepsz et al. in 2000, can be thought of as complementary to OE [66]. It is the ratio between any 60-s interval of renal activity during a given time and the first 60–120 s of the study. NORA can be calculated at any point during the study regardless of whether diuretic has been given. Typical acquisition times are at the end of the renogram, the end of the furosemide test, and after voiding. In other words, while OE describes what has left the kidney, NORA describes what remains behind.

Normal values were described in *Piepsz's* study comparing NORA values to OE in 175 normal kidneys and 82 postoperative dilated but not obstructed kidneys. As expected, *NORA in normal kidneys at 20 min was almost always <1.0* because normal adequate drainage has already occurred. When NORA is plotted versus OE values obtained at 20 min, there is an excellent linear correlation ($R^2 = -0.917$), which further confirms the complementary nature of the two parameters. Of note, the choice of background correction plays a role in NORA calculations with perirenal or subrenal background ROIs making up 67 or 83 % of the value obtained without background correction. Therefore, background correction should be standardized when reporting this parameter [67]. NORA has been found to be less robust than OE in patients with diminished renal function [68]. The results of this new quantitative parameter are interesting and potentially useful, but further study is required to compare values in patients with known obstruction.

Radionuclide Cystography

Traditionally, VCUG utilizing fluoroscopy has been the standard for the initial diagnosis of vesicoureteral reflux. In an effort to minimize radiation exposure, Winter introduced direct radionuclide cystography in 1959 [69]. Because image resolution is inferior to that of VCUG and precise grading is not possible, most centers in the United States use radionuclide cystography selectively. In a survey of North American pediatric urologists, Ellison et al. reported that only 1–3 % of those polled routinely ordered radionuclide cystography for children with antenatal hydronephrosis or after a first febrile UTI compared with 97–99 % who ordered VCUG. Radionuclide cystography was, however, utilized more frequently in the setting of vesicoureteral reflux follow-up (44 %) and in sibling screening (29 %) [70].

Direct Radionuclide Cystography

Access to the bladder is made sterilely either by urethral catheter (5–8 Fr), by Foley catheter with a deflated balloon during the voiding portion of the study, or by direct percutaneous suprapubic injection [71]. ^{99m}Tc-Pertechnate is the most commonly used radiotracer, but ^{99m}Tc-sulfur colloid or ^{99m}Tc-DTPA should be used in children with augmented bladders as these compounds are not absorbed via the bowel mucosa used in the augmentation [72]. The administered dose (0.5–1.0 mCi/kg) is the same for all three tracers. The radiotracer is mixed in 250–500 mL of sterile saline and hung approximately 70–100 cm above the table. Filling is complete when the age-appropriate volume is reached or upon cessation of flow from the bottle of solution.

The gamma camera is placed under the supine patient during the filling phase, and computer images are obtained at 5 s/frame. Once filling is complete, the cooperative patient is positioned upright with the camera posterior. Computer images are obtained every 2–10 s, and analog images are taken every 30–60 s. Pre- and postvoid bladder images are taken, and regions of interest are drawn around the bladder to calculate the postvoid residual.

The presence and duration of reflux, and if possible the estimated bladder volume during reflux, are reported. Grading is categorized as *mild*, tracer only in the ureter; *moderate*, tracer in a nondilated collecting system and ureter; and *severe*, tracer within a dilated collecting system and ureter (Fig. 6.8). Some authors have attempted to correlate reflux with bladder volumes and voiding with limited success [73, 74].

Acknowledged sources of error include inadequate bladder drainage in smaller caliber catheters, leakage of urine (and tracer) around the

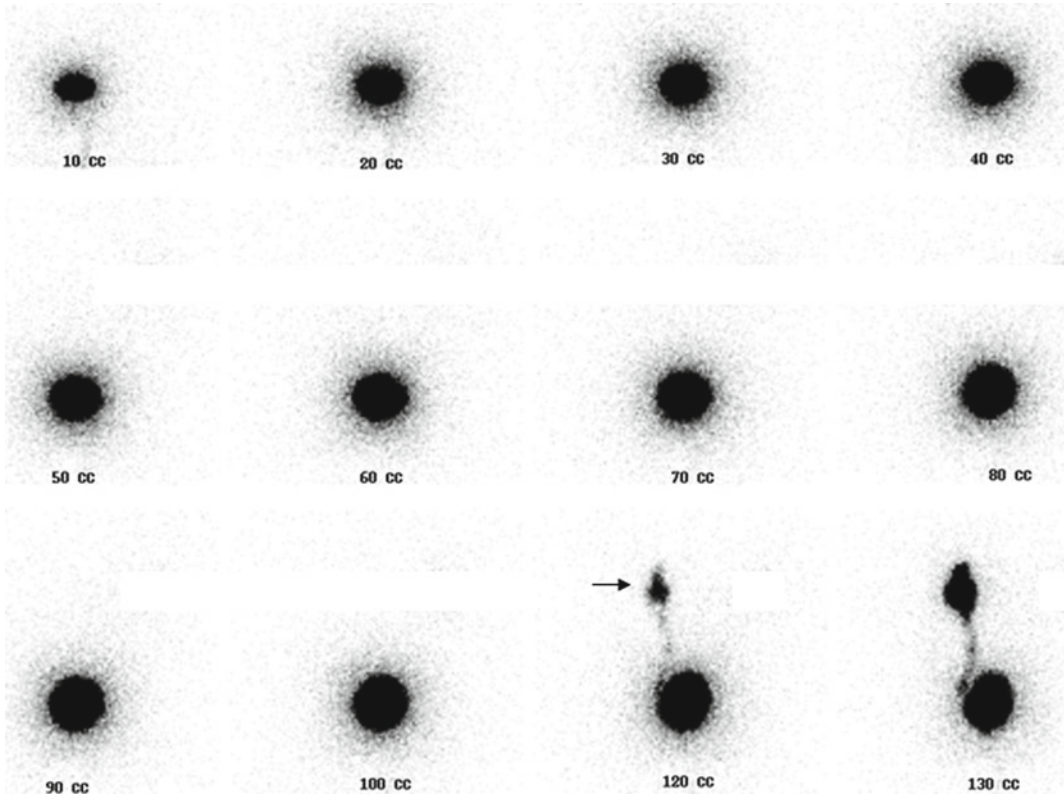

Fig. 6.8 Severe vesicoureteral reflux on direct radionuclide cystography. Activity extending into a dilated left pelvis/collecting system (*arrow*) can be appreciated when the urinary bladder volume is 120 cm^3

catheter, and skin contamination by urine. The latter two may result in false-positive exams.

Percutaneous Direct Radionuclide Cystography Technique

This technique, proposed by Wilkinson et al. in 2002, was aimed for use in older, toilet-trained children who seek to avoid the discomfort of urethral catheterization [71, 75]. EMLA or topical lidocaine is applied to the suprapubic area of puncture 45 min prior to initiation of the study. The child is encouraged to drink liquids, and bladder fullness is assessed by ultrasound. Ultrasound is also used to measure the distance between the skin and bladder, if less than 12 mm a 25 gauge needle can be used to inject the radiotracer directly into the full bladder. Larger needles may be necessary in older or more obese children.

Indirect Radionuclide Cystogram

The indirect radionuclide cystogram relies on patient cooperation to a much greater extent than direct cystography. As there is no urethral catheterization, the child must be able to voluntarily void and must remain still, or the test cannot be completed. The radiotracer of choice is ^{99m}Tc-MAG3, but ^{99m}Tc-DTPA can also be used at a dose of 0.08–0.12 mCi, administered either via venipuncture or IV catheter. Indirect cystography requires a conventional dynamic renal scan prior to the voiding phase of the study.

The child is placed supine with the camera posterior. Images are acquired at 1–4-s intervals for the first minute, followed by images at 1–5-min intervals for 30–60 min or until at least 80 % of the tracer has left the collecting system and entered the bladder. If necessary, the child can be positioned upright to aid in kidney drainage prior to voiding images. For the voiding phase, the child is asked to sit, and the camera is again placed posterior. When the child reports the urge to void, 2–10-s computer images are obtained until the end of voiding. Any patient movement during image acquisition can lead to spurious results. Of note, reflux can only be detected during the voiding phase, and if the patient cannot void, the test cannot be interpreted.

Direct Radionuclide Cystography Versus VCUG

Early studies suggest that DRC is comparable to VCUG in the detection of VUR and may be slightly more sensitive. Agreement between DRC and VCUG has been reported to be around 80 % with DRC detecting 17 % of cases missed by VCUG [76–78]. Kogan et al. report several cases of clinically significant VUR detected only on DRC and missed by VCUG in a highly selected population. They recommend supplemental DRC in those children with negative VCUG who have a clinical history of multiple febrile UTIs and/or cortical imaging suggestive of renal scarring due to occult reflux [78]. McLaren et al. found DRC to be even more sensitive than VCUG when prospectively examining infants presenting with febrile UTI. Each patient underwent both diagnostic studies yielding a sensitivity of 45 % for VCUG and 91 % for DRC. However, DRC missed half of grade 1, 20 % of grade 2, and 6 % of grade 3 VUR found on VCUG [79].

Direct Radionuclide Cystography Versus Indirect Radionuclide Cystography

Due to the nature of IRC, which relies on bladder filling after a dynamic renogram, only the voiding and postvoiding phases can be interpreted. The injected radiotracer must be cleared from the blood and excreted by the kidneys, and only after tracer has exited the collecting system and ureters can the study begin. Early reflux can potentially be masked by tracer already present in the ureter, or conversely ureteral tracer from the drainage phase could be interpreted as VUR. This significant limitation to the technique may potentially lead to false-negative or false-positive results. Early reports comparing the two tests confirm this concern. In a study of 137 patients

who underwent concurrent DRC and IRC, Conway et al. reported that 21 % of cases of VUR occurred only during the filling phase and would not be detectable by IRC [80].

Despite the logistical advantages (ease of interpretation, decreased radiation dose) of DRC versus IRC, many centers in Europe and Australia prefer IRC because it avoids urethral catheterization despite decreased sensitivity and specificity versus VCUG or DRC. When compared to VCUG as the standard, sensitivities range from 41 to 82 % and specificities from 44 to 90 % [81–86].

Percutaneous Direct Radionuclide Cystography Versus IRC and VCUG

In Wilkinson's report proposing suprapubic injection of radiotracer, 94 % of injections were successful in one attempt, and approximately 82 % of patients reported the suprapubic injections caused less discomfort than the IV placement required for IRC. Detection of reflux by PDRC was approximately half that of previously reported by IRC in the same patients (28 % vs. 66 %), but 30 % of the patients studied by PDRC had previously undergone corrective surgery for their reflux. Additionally, PDRC was performed in most cases up to a year after the initial IRC, thus allowing some cases of VUR to potentially resolve [71]. Jose et al. reported slightly better results in a more carefully selected patient population with VCUG and PDRC concordant in 90 %. *Sensitivity, specificity, and accuracy compared to VCUG were 76 %, 100 %, and 92 %*, respectively. Given its feasibility and excellent patient tolerability, it seems to be a technique that warrants further study, especially in older children who seek to avoid catheterization [75].

Scrotal Scintigraphy

Differentiating testicular torsion from epididymo-orchitis relying solely on clinical judgment can be quite challenging and often results in unnecessary scrotal exploration. Scrotal scintigraphy, first introduced in 1973 by Nadel et al. [87] to evaluate acute testicular pain, for many years was used as a first-line diagnostic modality to distinguish testis ischemia from inflammatory processes. More recently, color and power Doppler ultrasonography has been shown to be a powerful and noninvasive tool for evaluating testicular blood flow that does not involve ionizing radiation. This has obviated the need for scrotal scintigraphy in most situations. Several authors advocate combined ultrasonography and scrotal scintigraphy in equivocal cases.

Scrotal Scintigraphy Technique

^{99m}Tc-Pertechnate is given intravenously at a dose of 0.1 mCi/kg, with a minimum dose of 2 mCi and a maximum dose of 15 mCi. To prevent tracer uptake by the thyroid gland, 6 mg/kg of potassium perchlorate is given orally prior to the study. The patient is placed supine and the penis is secured superiorly and the scrotum is gently elevated above the thighs. The exam is then performed in two phases, angiography and static scintigraphy.

Tracer is given IV as a rapid bolus, and a low-energy collimator is used to record one frame per second for 60 s for the flow phase. After the flow phase is completed and without moving the camera, a single static image of the scrotum is obtained for 300,000–500,000 counts. A lead apron is placed over the thighs and under the scrotum to minimize background interference, and another lead apron is placed over the suprapubic area to obscure any bladder activity. Once appropriately shielded, another anterior static image is acquired using a pinhole collimator for 150,000 counts. If necessary, a cobalt 57 line source, or lead strip, may be placed in the midline to delineate the scrotal raphe.

Interpretation of Scrotal Scintigraphy

Normally, tracer activity is rarely seen in the scrotum during the flow phase of the study due to the relatively low blood flow in the area. Instead,

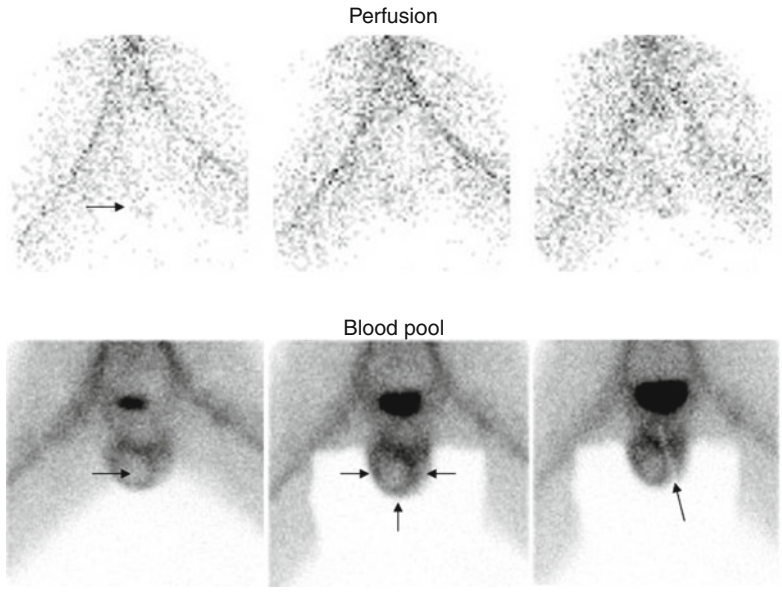

Fig. 6.9 Late testicular torsion. An 11-year-old boy presented with a 3-day history of right scrotal pain. There is mildly increased blood flow (*arrow*) to the right hemiscrotum on the perfusion (flow) phase of the study. On the blood-pool phase, in the near *left image*, there is a discrete photopenic defect (*arrow*) in the right hemiscrotum. There is a hyperemic rim (*arrows*, *center image*) surrounding this region. This is the typical presentation of late torsion. On the far *right image*, a lead shield has been placed on the median raphe (*arrow*), to help distinguish the right and left halves of the scrotum. A necrotic right testis was removed at surgery

tracer is more often visualized in the iliac and femoral vessels and in the soft tissue of the thighs. The static images should show symmetric uniform tracer uptake in the scrotum.

During *early acute torsion (<24 h)*, the flow phase often is normal, but on static images, there is reduced or absent uptake in the affected hemiscrotum. After a few hours of symptoms, there is sometimes a rim of increased tracer uptake surrounding the involved testicle.

In *late torsion (>24 h)*, the flow phase may show a central region of decreased or absent activity corresponding to the affected testis. There can also be a peripheral rim of increased activity. Static images also show a similar pattern of decreased or absent activity surrounded by an area of increased activity (Fig. 6.9).

In contrast to testicular torsion, *inflammatory processes such as epididymitis and orchitis* will appear as increased activity on both the flow and static images (Fig. 6.10). An abscess may have an appearance similar to that of late testicular torsion. The often irregular border of an abscess and a rim of hyperperfusion that is not always completely circumferential may help to differentiate this condition from late torsion.

Torsion of the epididymal appendage is rarely if ever demonstrated on scrotal scintigraphy as it lacks the necessary resolution. A torsed appendage can appear as normal or increased flow on the flow phase and appears as normal on the static image. However, the aim of study is to exclude testicular torsion.

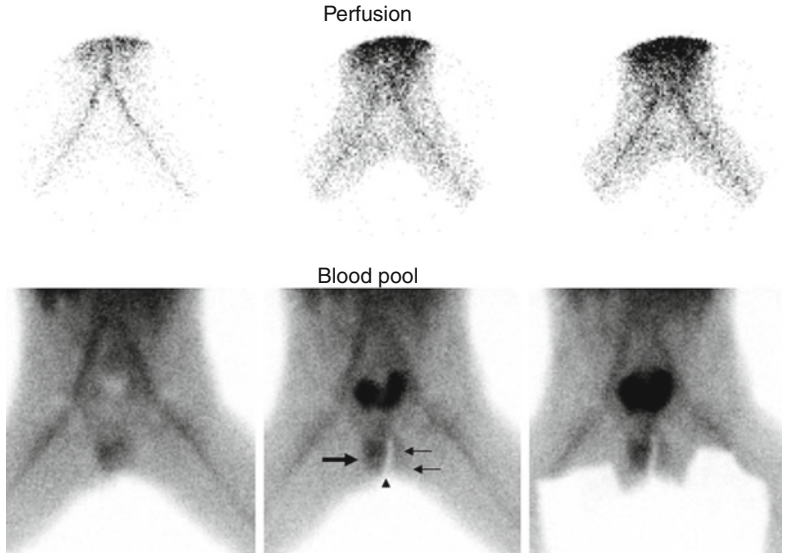

Fig. 6.10 Inflammation. A 4-year-old boy presented with a 4-day history of right scrotal pain. There is very mild hyperperfusion to the right hemiscrotum on the perfusion phase of the study. On the blood-pool images, there is diffusely increased activity throughout the right hemiscrotum (*thick arrow*). Compare with the left hemiscrotum (*arrows*). A lead strip has been placed on the median raphe (*arrowhead*)

References

1. Enlander D, Weber PM, dos Remedios LV. Renal cortical imaging in 35 patients: superior quality with 99Tc-DMSA. J Nucl Med. 1974;15:743–9.
2. Peters AM, Jones DH, Evans K, et al. Two routes for 99mTc-DMSA uptake into the renal cortical tubular cell. Eur J Nucl Med. 1988;14:555–61.
3. de Lange MJ, Piers DA, Kosterink JG, et al. Renal handling of 99mTc-DMSA: evidence for glomerular filtration. J Nucl Med. 1989;30:1219–23.
4. Kawamura J, Hosokawa S, Yoshida O, et al. Renal function studies using 99mTc-DMSA. Clin Nucl Med. 1979;4:39–46.
5. Durand E, Prigent A. Can dimercaptosuccinic acid be used to assess global renal function? Eur J Nucl Med. 2000;27(7):727–9.
6. Krill A, Cubillos J, Gitlin J, et al. Abdominopelvic ultrasound: a cost-effective way to diagnose solitary kidney. J Urol. 2012;187:2201–4.
7. Itoh K. 99mTc-MAG3: review of pharmacokinetics, clinical application to renal diseases and quantification of renal function. Ann Nucl Med. 2001;15(3):179–90.
8. Al-Nahhas AA, Jafri RA, Britton KE, et al. Clinical experience with 99mTc-MAG3, mercaptoacetyltriglycine, and a comparison with 99mTc-DTPA. Eur J Nucl Med. 1988;14:453–62.
9. Bubeck B, Brandau W, Steinbacher M, et al. Technetium-99m labeled renal function and imaging agents: II. Clinical evaluation of 99mTc-MAG3. Int J Rad App Instrum B. 1988;15:109–18.
10. Taylor A, Eshima D, Alazraki N. 99mTc-MAG3, A new renal imaging agent: preliminary results in patients. Eur J Nucl Med. 1987;12:510–14.
11. Ritchie G, Wilkinson AG, Prescott RJ. Comparison of differential renal function using 99mTc-MAG3 and 99mTc-DMSA renography in a paediatric population. Pediatr Radiol. 2008;38:857–62.
12. Gordon I, Anderson PJ, Lythgoe MF, et al. Can 99mTc-MAG3 replace 99mTc-DMSA in the exclusion of a focal renal defect? J Nucl Med. 1992;33:2090–3.
13. Bair HJ, Becker W, Schott G, et al. Is there still a need for 99mTc-DMSA renal imaging? Clin Nucl Med. 1995;20:18–21.
14. Hauser W, Atkins HL, Nelson KG, et al. 99mTc-DTPA: a new radiopharmaceutical for brain and kidney scanning. Radiology. 1970;94:679–84.
15. Klopper JF, Hauser W, Atkins HL, et al. Evaluation of 99mTc-DTPA for the measurement of GFR. J Nucl Med. 1972;13:107–10.
16. Taylor A, Nally JV. Clinical applications of renal scintigraphy. Am J Roentgenol. 1995;164:31–41.
17. Taylor A, Clark S, Ball T. Comparison of 99mTc-MAG3 and 99mTc-DTPA scintigraphy in neonates. Clin Nucl Med. 1994;19:575–80.
18. Smith T, Gordon I, Kelly JP. Comparison of radiation dose from intravenous pyelography and 99mTc-DMSA scintigraphy in children. Br J Radiol. 1998;71:314–19.
19. Stabin MG. In: Treves ST, editor. Pediatric nuclear medicine. 2nd ed. Internal Dosimetry in Pediatric Nuclear Medicine. New York: Springer; 1995. p. 556–78.

20. Ward VL, Strauss KJ, Barnewolt CE, et al. Pediatric radiation exposure and effective dose reduction during voiding cystourethrography. Radiology. 2008; 249(3):1002–9.
21. Braren V, Versage PN, Touya JJ, et al. Radioisotopic determination of glomerular filtration rate. J Urol. 1979;121:145–7.
22. Klopper JF, Hauser W, Atkins HL, et al. Evaluation of 99mTc-DTPA for the measurement of glomerular filtration rate. J Nucl Med. 1972;13:107–10.
23. Gates GF. Glomerular filtration rate: estimation from fractional renal accumulation of 99mTc-DTPA (Stannous). AJR Am J Roentgenol. 1982;138:565–70.
24. Koff SA, McDowell GC, Byard M. Diuretic radionuclide assessment of obstruction in the infant. J Urol. 1988;140:1167.
25. Gonzalez R, Chiou RK. The diagnosis of upper urinary tract obstruction in children: comparison of diuresis renography and pressure flow studies. J Urol. 1985;133:646–9.
26. Chandhoke PS, Kogan BA, Al-Dahwi A, et al. Monitoring renal function in children with urological abnormalities. J Urol. 1990;144:601–5.
27. Hansson S, Dhamey M, Sigstrom O, et al. DMSA scintigraphy instead of voiding cystourethrography for infants with urinary tract infection. J Urol. 2004;172:1071–4.
28. Pohl HG, Belman AB. The "top-down" approach to the evaluation of children with febrile UTI. Adv Urol. 2009: 1–5.
29. Prigent A, Cosgriff P, Gates G, et al. Consensus on quality control of quantitative measurements from the renogram: International Consensus Committee from the Scientific Committee of Radionuclides in Nephrourology. Semin Nucl Med. 1999;29(2):146–59.
30. Piepsz A, Blaufox MD, Gordon I, et al. Consensus on renal cortical scintigraphy in children with UTI. Semin Nucl Med. 1999;29(2):160–74.
31. Zeissman HA, Majd M. Importance of methodology on 99mTc-DMSA image quality: imaging pilot study for RIVUR multicenter investigation. J Urol. 2009;182:272–9.
32. Applegate KE, Connolly LP, Davis RT, et al. A prospective comparison of high resolution planar, pinhole and triple detector SPECT for the comparison of renal cortical defects. Clin Nucl Med. 1997; 22(10):673–8.
33. Rodriguez JL, Perera A, Fraxedas R, et al. Renal 99mTc-DMSA SPET and planar imaging: are they really the same? Nucl Med Commun. 1997;18:556.
34. Rossleigh MA, Farnsworth RH, Leighton DM, et al. 99mTc-DMSA scintigraphy studies of renal cortical scarring and length. J Nucl Med. 1998;39(7):1280–5.
35. Treves ST, Majd MM, Kuruc A, et al. Pediatric nuclear medicine. 2nd ed. Chapter 17. New York: Springer; 1995. p. 339–99.
36. Yen TC, Chen WP, Chang SL, et al. 99mTc-DMSA renal SPECT in diagnosing and monitoring pediatric acute pyelonephritis. J Nucl Med. 1996;37(8):1349–53.
37. Majd M, Rushton HG, Chandra R, et al. 99mTc-DMSA renal cortical scintigraphy to detect experimental acute pyelonephritis in piglets: comparison of planar (pinhole) and SPECT imaging. J Nucl Med. 1996;37(10):1731–4.
38. De Sadeleer C, Tondeur M, Melis K, et al. A multicenter trial on interobserver variability in reporting on 99mTc-DMSA planar scintigraphy: a Belgian survey. J Nucl Med. 2000;41(1):23–6.
39. Gacinovic S, Buscome J, Costa DC, et al. Interobserver agreement in the reporting of Tc-99m DMSA renal studies. Nucl Med Commun. 1996;17:596.
40. Craig JC, Irwig L, Ford M, et al. Reliability of DMSA for the diagnosis of renal parenchymal abnormality in children. Eur J Nucl Med. 2000;27(11):1610–16.
41. Craig JC, Wheeler DM, Irwig L, et al. How accurate is DMSA scintigraphy for the diagnosis of acute pyelonephritis? A meta-analysis of experimental studies. J Nucl Med. 2000;41(6):986–93.
42. Rushton HG, Majd M, Chandra R, et al. Evaluation of 99mTc-DMSA renal scan in experimental acute pyelonephritis in piglets. J Urol. 1998;140:1169–74.
43. Verboven M, Ingels M, Delree M, et al. 99mTc-DMSA scintigraphy in acute UTI in children. Pediatr Radiol. 1990;20:540–2.
44. Tarkington M, Fildes RD, Levin K, et al. High resolution SPECT 99mTC-DMSA renal imaging: a state of the art technique. J Urol. 1990;144:598–600.
45. Peters C, Mandell J, Treves T, et al. The "well tempered" diuretic renogram: a standard method to examine the asymptomatic neonate with hydronephrosis or hydroureteronephrosis. J Nucl Med. 1992;33(11):2047–51.
46. Mandell GA, Cooper JA, Leonard JC, et al. Procedure guidelines for diuretic renography in children. J Nucl Med. 1997;38(10):1647–9.
47. Lythgoe MF, Gordon I, Anderson PJ. The effect of renal maturation on the clearance of 99mTc-MAG3. Eur J Nucl Med. 1994;21(12):1332–7.
48. Gordon I, Piepsz A, Sixt R. Guidelines for standard and diuretic renogram in children. Eur J Nucl Med. 2011;38:1175–88.
49. Nguyen HT, Gluckman GR, Kogan BA. Changing the technique of background subtraction alters calculated renal function on pediatric MAG3 renography. J Urol. 1997;158:1252–6.
50. Ozcan Z, Anderson PJ, Gordon I. Robustness of estimation of differential renal function in infants and children with unilateral prenatal diagnosis of a hydronephrotic kidney on dynamic renography: how real is the supranormal kidney? Eur J Nucl Med Mol Imaging. 2006;33(6):738–44.
51. Oh SJ, Moon DH, Kang WC, et al. Supranormal differential renal function is real but May Be pathological: assessment by ^{99m}Technetium mercaptoacetyltriglycine renal scan of congenital unilateral hydronephrosis. J Urol. 2001;165:2300–4.
52. Capolicchio G, Jednak R, Dinh L, et al. Supranormal renographic differential function in congenital hydronephrosis: fact, not artifact. J Urol. 1999;161:1290.

53. Inanir S, Biykli N, Caliskan B, et al. Contradictory supranormal function in hydronephrotic kidneys: fact or artifact on pediatric MAG3 renal scans? Clin Nucl Med. 2005;30(2):91–6.
54. Gungor F, Anderson P, Gordon I. Effect of the size of regions of interest on the estimation of differential renal function in children with congenital hydronephrosis. Nucl Med Commun. 2002;23:147–51.
55. Piepsz A. Antenatal detection of pelviureteric junction stenosis: main controversies. Semin Nucl Med. 2011;41:11–9.
56. O'Reilly PH, Testa HJ, Lawson RS, et al. Diuresis renography in equivocal urinary tract obstruction. Br J Urol. 1978;50:76–80.
57. O'Reilly PH, Lawson RS, Shields RA, et al. Idiopathic hydronephrosis-the diuresis renogram: a New Non-invasive method of assessing equivocal pelvioureteral junction obstruction. J Urol. 1979;121:153–5.
58. Ransley PG, Dhillon HK, Gordon I, et al. The postnatal management of hydronephrosis diagnosed by prenatal ultrasound. J Urol. 1990;144:584.
59. Ulman I, Jayanthi VR, Koff SA. The long-term follow-up of newborns with severe unilateral hydronephrosis initially treated nonoperatively. J Urol. 2000;164:1101–5.
60. Ross SS, Kardos S, Krill A, et al. Observation of infants with SFU grades 3–4 hydronephrosis: worsening drainage with serial diuresis renography indicates surgical intervention and helps prevent loss of renal function. J Pediatr Urol. 2011;7:266–71.
61. Rossleigh MA, Thomas MY, Moase AL. Determination of the normal range of furosemide half-clearance times when using MAG3. Clin Nucl Med. 1994;19:880–2.
62. Rossleigh MA, Leighton DM, Farnsworth RH. Diuretic renography: the need for an additional view after gravity assisted drainage. Clin Nucl Med. 1993;18:210–13.
63. Wong DC, Rossleigh MA, Farnsworth RH. Diuretic renography with the addition of quantitative gravity-assisted drainage in infants and children. J Nucl Med. 2000;41(6):1030–6.
64. Chaiwatanarat T, Padhy AK, Bomaji JB, et al. Validation of renal output efficiency as an objective parameter in the evaluation of upper urinary tract obstruction. J Nucl Med. 1993;34(5):845–8.
65. Saunders CAB, Choong KL, Larcos G, et al. Assessment of pediatric hydronephrosis using output efficiency. J Nucl Med. 1997;38(9):1483–6.
66. Piepsz A, Tondeur M, Ham H. NORA: a simple and reliable parameter for estimating renal output with or without furosemide challenge. Nucl Med Commun. 2000;21:317–23.
67. Piepsz A, Kuyvenhoven JD, Tondeur M, et al. Normalized residual activity: usual values and robustness of the method. J Nucl Med. 2002;43(1):33–8.
68. Nimmon CC, Samal M, Britton KE. Elimination of total renal function on renal output efficiency and normalized residual activity. J Nucl Med. 2004;45(4):587–93.
69. Winter CC. A new test for vesicoureteral reflux: an external technique using radioisotopes. J Urol. 1959;81:105–11.
70. Ellison JS, Maxfield CM, Wiener JM. Voiding cystography practices of North American pediatric urologists. J Urol. 2009;182:299–305.
71. Wilkinson AG. Percutaneous direct radionuclide cystography in children: description of technique and early experience. Pediatr Radiol. 2002;32:511–17.
72. Mandell GA, Eggli DF, Gilday DL, et al. Procedure guideline for radionuclide cystography in children. J Nucl Med. 1997;38(10):1650–4.
73. McLaren CJ, Simpson ET. Direct comparison of radiology and nuclear medicine cystograms in young infants with vesico-ureteral reflux. BJU Int. 2001;87:93–7.
74. Mozley PD, Heyman S, Duckett JW, et al. Direct vesicoureteral scintigraphy: quantifying early outcome predictors in children with primary reflux. J Nucl Med. 1994;35(10):1602–8.
75. Jose TE, Mohiudheen H, Patel C, et al. Direct radionuclide cystography by suprapubic puncture: comparison with voiding cystourethrography. Nucl Med Commun. 2004;25(4):383–5.
76. Nasrallah PF, Nara S, Crawford J. Clinical applications of nuclear cystography. J Urol. 1982; 128:550–3.
77. Sukan A, Bayazit AK, Kibar M, et al. Comparison of direct radionuclide cystography and voiding direct cystography in the detection of vesicoureteral reflux. Ann Nucl Med. 2003;17(7):549–53.
78. Kogan SJ, Sigler L, Levitt SB, et al. Elusive vesicoureteral reflux in children with normal contrast cystograms. J Urol. 1986;136:325–8.
79. McLaren CJ, Simpson ET. Vesico-ureteral reflux in the young infant with follow-up direct radionuclide cystograms: the medical and surgical outcome at 5 years old. BJU Int. 2002;90:721–4.
80. Conway JJ. Kruglik. Effectiveness of direct and indirect radionuclide cystography in detecting vesicoureteral reflux. J Nucl Med. 1976;17(2):81–3.
81. Merrick MV, Uttley WS, Wild R. A comparison of Two techniques in detecting vesicoureteral reflux. Br J Radiol. 1979;50:792–5.
82. Nielsen JB, Jensen FT, Munch JT, et al. The diagnosis of VUR- radiologic and nuclear medicine methods. Scand J Urol Nephrol. 1985;19:109–12.
83. Carlsen O, Lukman B, Nathan E. Indirect radionuclide reno-cystography for determination of vesicoureteral reflux in children. Eur J Nucl Med. 1986; 12:205–10.
84. Chapman SJ, Chantler C, Haycock GB, et al. Radionuclide cystography in vesicoureteral reflux. Arch Dis Child. 1988;63:650–1.
85. Gordon I, Peters M, Morony S. Indirect radionuclide cystography: a sensitive technique for the detection of vesico-ureteral reflux. Pediatr Nephrol. 1990;4:604–6.
86. DeSadeleer C, DeBoe V, Desprechins B, et al. How good is 99mTc-MAG3 indirect cystography? Eur J Nucl Med. 1994;21(3):223–7.

87. Nadel NS, Gitter MH, Hahn LC, et al. Pre-operative diagnosis of testicular torsion. Urology. 1973;1:478.
88. Gadd R, Mountford PJ, Oxtoby JW. Effective dose to children and adolescents from radiopharmaceuticals. Nucl Med Commun. 1999;20:569.
89. Fotakis M, Athansopoulou EM, Psarrakos K, et al. Radiation doses to paediatric patients up to 5 years of age undergoing micturating cystourethrography examinations and its dependence on patient age: a Monte Carlo study. BR J Radiol. 2003;76:812.